

Discriminating volcano deformation due to magma movements and variable surface loads: application to Katla subglacial volcano, Iceland

V. Pinel,¹ F. Sigmundsson,² E. Sturkell,² H. Geirsson,³ P. Einarsson,⁴
M. T. Gudmundsson⁴ and T. Högnadóttir⁴

¹IRD, UMR 5559, Chambéry, France, Laboratoire de Géophysique Interne et Tectonophysique, Université de Savoie, Campus Scientifique, 73376 Le Bourget du Lac Cedex, France. E-mail: Virginie.Pinel@univ-savoie.fr

²Nordic Volcanological Center, Institute of Earth Sciences, Askja, University of Iceland, Sturlugata 7, IS-101 Reykjavik, Iceland

³Icelandic Meteorological Office, Reykjavik, Iceland

⁴Institute of Earth Sciences, Askja, University of Iceland, Sturlugata 7, IS-101 Reykjavik, Iceland

Accepted 2006 October 13. Received 2006 September 11; in original form 2006 February 1

SUMMARY

Surface displacements induced by ice load variation through time are calculated by spatial integration of Green's function for both end-members: an elastic half-space and a thick elastic plate lying over an inviscid mantle. The elastic half-space model allows the consideration of displacements caused by short-term (seasonal) variations. The thick plate model describes the final relaxed state. The transition between these two stages is dominated by an effective relaxation time which depends on mantle viscosity. This behaviour is considered to estimate displacements induced by long-term load changes (ice retreat over decades). We apply these methods to the Mýrdalsjökull ice cap, Iceland, where an annual cycle in ice load occurs as well as a gradual ice retreat as a consequence of climate warming. Seasonal vertical displacements measured from 2000 to 2006 at two continuous GPS stations located near the edge of Mýrdalsjökull ice cap fit well to a model of an elastic response to the annual variation in ice load. A comparison of model displacements and observations provides a minimum value of 29 ± 5 GPa for the effective static local value of the Young's modulus. We infer long-term displacements induced by ice retreat over the last 115 yr using a combination of the instantaneous elastic response and the final relaxed state. Results are compared to GPS measurements used to monitor the Katla volcano lying beneath the Mýrdalsjökull ice cap. A forward model considering an elastic thickness of 5 km can explain a fraction of the uplift recorded from 1999 to 2004, but it cannot account for the observed horizontal velocities. The study confirms that magma inflow is required to explain observed inflation of the Katla volcano 1999–2004.

Key words: crustal deformation, GPS, Green's function, retreating ice cap, seasonal effects on volcanoes.

1 INTRODUCTION

Crustal deformation at volcanoes is frequently related to subsurface magmatic movements, such as volcano inflation due to magma accumulation prior to eruptions. Other processes may, however, contribute as well. In this paper we explore what role subtle load changes may have on geodetic measurements at volcanoes, in particular the influence of ice load changes at subglacial volcanoes. This is of particular concern as many of the world's volcanoes are topped by glaciers, which volume varies considerably over time spans of years. Ongoing climate warming causes general retreat of small ice caps covering volcanoes, eventually leading to elastic or glacio-isostatic crustal adjustment causing uplift and horizontal displacements radiating away from the ice caps. In Iceland, uplift induced by historical

ice volume change at the largest ice cap, Vatnajökull (average radius of about 50 km), has been inferred e.g. by Sigmundsson & Einarsson (1992) and Pagli *et al.* (2005). Such signals at smaller ice caps with comparable spatial extent to underlying subglacial volcanoes can mistakenly be interpreted as inflation due to magma accumulation; alternatively in case of real magma accumulation at a subglacial volcano it is of importance to correctly relate the associated inflation to that process. One aim of this paper is therefore to develop techniques to discriminate deformation due to the ice unloading and magmatic processes at subglacial volcanoes. We apply the techniques to the subglacial Katla volcano in Iceland, which is believed to be near the end of its repose period and may receive inflow of magma. However, the volcano also sits under an ice cap that has been retreating in recent years. GPS-measurements

indicative of uplift and expansion at the volcano in the 2001–2004 period are evaluated in terms of the two suggested processes. Apparent annual cycle in deformation of the volcano is modelled as well in terms of an annual load change.

Load-induced deformation on volcanoes is in general likely to be affected by 3-D variation in rheology and crustal heterogeneities, such as those associated with magma chambers and their surroundings. A Maxwell viscoelastic behaviour with varying rheological parameters may be appropriate for the bulk of the crust. Fine-scale details in load history are, however, difficult to incorporate in such models, and local variations in crustal rheology remain poorly known. At Katla volcano, we have good knowledge about load changes and their spatial extent in recent years, but details of rheology and the underlying magmatic source are uncertain. We rely therefore on simplified earth models (with uniform rheology), but allow for the possibility of complicated load geometries on the surface of the Earth through the use of Green's functions. We model the initial response of the Earth to load on the surface as that of a load on an elastic half-space. The same approach has already been used to calculate stress field changes induced by partial destruction of volcanic edifices (Pinel & Jaupart 2005). However, in case of re-treating ice caps, the lateral extent of the relevant load may be of the same order or even larger than the effective elastic thickness of the lithosphere. It follows that the elastic response may only correspond to a short period of time following a load change. Viscous effect induced by the underlying mantle may contribute to the deformation as well. We model the final relaxed state of the Earth after loading as that of an elastic plate over a fully relaxed fluid. The transition between these two stages is dominated by an effective relaxation time for displacements.

2 MODEL DESCRIPTION

Loads on the surface of the Earth induce displacement fields which evolve through time. The long-term response to such loads can be approximated as the response to a load introduced on an elastic plate lying over a ductile material. The plate (corresponding to the relatively cold strong outermost layer of the Earth, behaving elastically over long timescales) is characterized by the elastic parameters: Poisson's ratio ν and Young's modulus E . The ductile material can be approximated as a Newtonian viscous fluid characterized by a density ρ_f , which determines the buoyancy force acting at the base of the elastic plate, and a viscosity η , which determines the temporal evolution of displacement.

We present calculations of surface displacements induced by a unit point mass applied at the surface for two end-member models: the elastic half-space (instantaneous response) and the elastic plate lying over an inviscid fluid (final response). A combination of these two cases gives the temporal evolution of displacements. The loads we consider are of limited spatial extent, warranting a flat Earth approximation. All calculations in this paper deal with perturbations from a reference lithostatic state before loading. In the following models, we will always consider the vertical axis (z) to be directed downwards so that unloading will mainly induce a negative vertical displacement.

2.1 Green's functions for the elastic half-space

Displacement of the surface induced by a unit point mass applied on an elastic half-space is given, in cylindrical coordinates, by Sneddon (1951) who solved the equations of the equilibrium ($\text{div}(\sigma) = 0$)

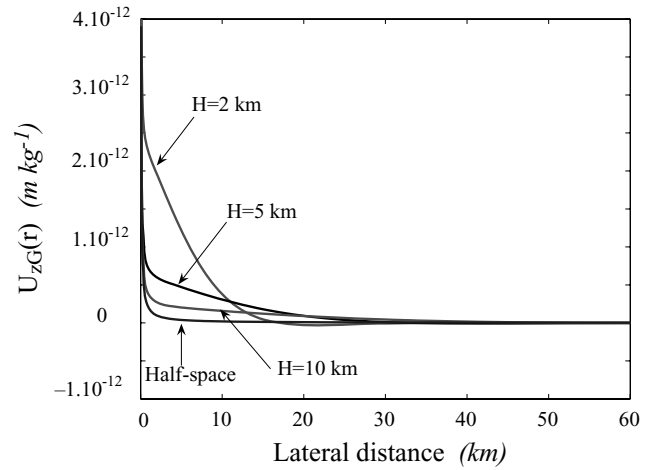


Figure 1. Vertical displacement as a function of lateral distance. Curves represent the value of U_{zG^∞} (half-space case) and U_{zGH} with $H = 2, 5$ and 10 km (thick plate case). Calculations are done with $\nu = 0.25$ and $E = 15$ GPa. The curve representing U_{zGH} for $H = 50$ km overlaps with the curve for the half-space.

for an axisymmetric load. Resulting radial (U_r) and vertical (U_z) displacements on the surface of the half-space as a function of distance (r) from the load are given as:

$$U_{rG^\infty}(r) = -\frac{g}{2\pi} \frac{(1+\nu)(1-2\nu)}{E} \frac{1}{r} \quad (1)$$

$$U_{zG^\infty}(r) = \frac{g}{\pi} \frac{1-\nu^2}{E} \frac{1}{r} \quad (2)$$

The buoyancy due to deflection of the top boundary is neglected. This unit point mass response is used as a Green's function (SI unit being m/kg). The displacement induced by any given distributed load is calculated by the convolution of this Green's function with the ice mass. The vertical displacement at point P (coordinates \vec{r}) is given by:

$$U_z^\infty(\vec{r}) = \int_R U_{zG^\infty}(\vec{r} - \vec{r}') \rho(\vec{r}') h(\vec{r}') dS(\vec{r}') \quad (3)$$

where ρ and h are, respectively, the density and the thickness of the load, $dS(\vec{r}')$ is an infinitesimal area of integration around point P and R is the area of the load. The horizontal displacement is obtained the same way except doing a vectorial integration. For a disc load, we checked that the convolution of the Green's function gave the same result as calculations by Pinel & Jaupart (2000). Displacements induced by a unit mass load applied on an elastic half-space are shown in Figs 1 and 2.

2.2 Green's functions for a thick elastic plate overlying an inviscid fluid

We now model the Earth as being made of an elastic layer of arbitrary thickness H lying over an inviscid fluid of density ρ_f , modelling the fully relaxed response of the Earth to load changes. We do not restrict our study to the thin plate approximation (where the vertical normal stress is set to zero (Comer 1983)), so we refer to it as a thick plate solution. We calculate the surface displacement induced by a unit point mass and solve for the equation of equilibrium ($\text{div}(\sigma) = 0$) in Lagrangian coordinates. Boundary conditions of this axisymmetric

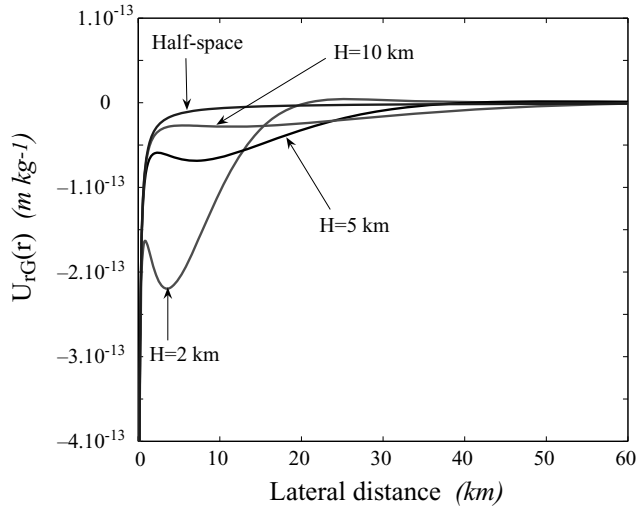


Figure 2. Radial displacement as a function of lateral distance. Curves represent the value of U_{rG^∞} (half-space case) and U_{rGH} with $H = 2, 5$ and 10 km (thick plate case). Calculations are done with $\nu = 0.25$ and $E = 15$ GPa. The curve representing U_{rGH} for $H = 50$ km overlaps with the curve for the half-space.

problem are expressed by (SI unit being Pa/kg):

$$\sigma_{zz}(r, z = 0) = g \lim_{a \rightarrow 0} \frac{\Pi_a(r)}{\pi a^2} \quad (4)$$

$$\sigma_{zz}(r, z = H) = g \rho_f U_z(r, z = H) \quad (5)$$

$$\tau_{rz}(r, z = 0) = 0 \quad (6)$$

$$\tau_{rz}(r, z = H) = 0 \quad (7)$$

with $\Pi_a(r) = 1$ for $0 \leq r \leq a$ and $\Pi_a(r) = 0$ for $r > a$. Our convention is such that a compression corresponds to a positive stress. Following Comer (1983) who calculated the effect of an harmonic load, we apply at the lower surface of the plate (at $z = H$) a pressure equal to the hydrostatic pressure in the fluid and no tangential component. In cylindrical coordinates, we use the method outlined by Sneddon (1951). Displacements are calculated by integrating Bessel function and are expressed, at the surface ($z = 0$) by:

$$U_{rGH}(r) = -\frac{g}{2\pi E(1-2\nu)} \int_0^\infty \left[(1-\nu^2) \left(2\epsilon \frac{A}{D} + 4\nu \right) \right] \times J_1(\epsilon r) d\epsilon + U_{rG^\infty} \quad (8)$$

$$U_{zGH}(r) = \frac{(1-\nu^2)g}{E\pi} \int_0^\infty \left[\frac{B}{D} - 1 \right] J_0(\epsilon r) d\epsilon + U_{zG^\infty} \quad (9)$$

where ϵ is a variable of integration, J_0 and J_1 are, respectively, the zeroth- and the first-order Bessel function of the first kind and coefficients A, B and D are defined by

$$A = \epsilon^2 H^2 - \nu(\cosh(2\epsilon H) - 1) - \frac{2(1-\nu^2)}{E} g \rho_f \left(\nu \frac{\sinh(2\epsilon H)}{\epsilon} + H \right) \quad (10)$$

$$B = \frac{1}{2} \epsilon \sinh(2\epsilon H) + \epsilon^2 H + \frac{1-\nu^2}{E} g \rho_f (\cosh(2\epsilon H) - 1) \quad (11)$$

$$D = -\epsilon^3 H^2 + \frac{1}{2} \epsilon (\cosh(2\epsilon H) - 1) + \frac{1-\nu^2}{E} g \rho_f (\sinh(2\epsilon H) + 2\epsilon H) \quad (12)$$

When $H \rightarrow \infty$, we have $(A/D) \rightarrow -\frac{2\nu}{\epsilon}$ and $(B/D) \rightarrow 1$ so that we find the solution for the elastic half-space given by eqs (1) and (2). Displacements induced by a unit mass load applied on a thick elastic plate are shown in Figs 1 and 2. This unit point mass response serves as a Green's function for the thick plate case and by convolution with the ice mass we find the displacement caused by any given distributed load. Similarly to eq. (3) vertical displacement is given by

$$U_z^H(\vec{r}) = \int_R U_{zGH}(\vec{r} - \vec{r}') \rho(\vec{r}') h(\vec{r}') dS(\vec{r}') \quad (13)$$

Brotchie & Silvester (1969) present a solution for the vertical displacement induced by a concentrated load on a plate but their result was obtained considering a thin plate. Comer (1983) shows that the thick plate calculation is different from the thin plate approximation for short wavelengths. In order to derive Green's function for concentrated load, the thick plate calculation seems more appropriate than the thin plate approximation. We used our Green's function to calculate the displacement induced by a uniform disc load. When the load radius is large enough compared to the plate thickness, our results are similar to the ones obtained by Brotchie & Silvester (1969). In that case the vertical displacement at the centre of the load approaches the isostatic equilibrium ($\rho_L H_L / \rho_f$) where ρ_L and H_L are the density and height of the load.

2.3 Ratio of horizontal and vertical displacement-comparison to magmatic deformation source

A convenient way to characterize the displacement field induced by a surface load change is to consider the ratio between induced horizontal and vertical displacements because the ratio is less sensitive to the crustal properties than the amplitude of displacements. For the instantaneous elastic response to a point source load, this ratio ($|U_{rG^\infty}(r)/U_{zG^\infty}(r)| = \frac{1-2\nu}{2(1-\nu)}$, which corresponds to a numerical value of 1/3 in case of $\nu = 0.25$) depends neither on the value of Young's modulus nor on the distance from the point load. For a given load distribution, the horizontal displacement is obtained by a vectorial integration (so that the norm is smaller or equal to the sum of the point load contributions) whereas the vertical displacement is obtained by a simple summation. It follows that the value of 1/3 corresponds to a upper limit for the ratio of the horizontal and vertical displacements for any distribution of load applied to an elastic half-space characterized by uniform Young's modulus E . For instance, the ratio between the modulus of horizontal displacement and the vertical one obtained for a uniform disc load is equal to 0 at the centre of the load and it increases with lateral distance until it reaches the limit value of $|U_{rG^\infty}(r)/U_{zG^\infty}(r)|$. Far enough from the load, the disc is seen as a concentrated load. The limit value is reached at a lateral distance around three times the radius of the load, as shown in Fig. 3.

In case of a concentrated load applied on a thick elastic plate lying above an inviscid medium, the ratio between horizontal and vertical displacement depends on the lateral position, the Young's modulus and the plate thickness. Results are shown in Fig. 4 (continuous curves) for different plate thickness considering a Young's modulus

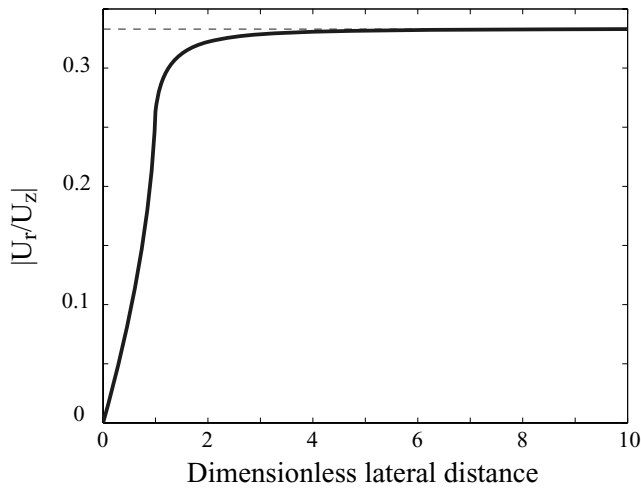


Figure 3. Ratio between radial and vertical displacements for a disc load (radius R) applied on an elastic half-space. Ratio is given as a function of the dimensionless lateral distance (r/R). Value of parameter ν is fixed at 0.25. At large distance, this ratio tends to the value of $|U_{rG^\infty}|/|U_{zG^\infty}| = 1/3$.

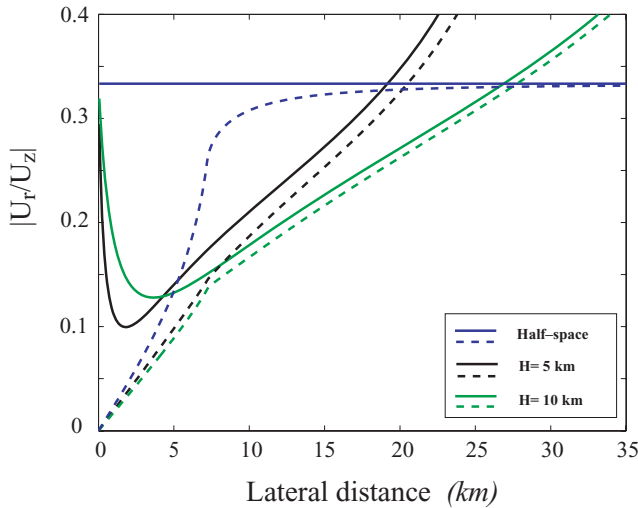


Figure 4. Ratio between radial and vertical displacements as a function of the lateral distance. Continuous curves correspond to the displacement induced by a unit point mass, dashed curves correspond to a 7 km radius uniform disc load. The different colours correspond to different elastic thickness. Value of parameter ν is fixed at 0.25 and $E = 15$ GPa.

of 15 GPa. At distances less than 10 km from the concentrated load this ratio is smaller than the value of $1/3$ but further away it can increase above this value. The value of $1/3$ is reached, at respectively, 11.5, 19 and 27 km for plates thickness of $H = 2, 5$ and 10 km. Similarly as for the elastic case, the ratio $|U_{rG^H}|/|U_{zG^H}|$ gives a maximum value for the ratio of displacement induced by any distribution of surface load applied on a thick plate because $|U_{rG^H}|$ is the horizontal displacement induced in the direction away from the load. In Fig. 4, values for the disc load (dashed curves) are always smaller than the corresponding values for the unit point mass (continuous curves).

For any volcano with deformation suspected to originate from both magma movements at depth and load changes on the surface, an immediate concern is how to discriminate the two. We have shown that ratio of horizontal and vertical displacement during unloading is

to some extent relatively independent of the parameters of the earth models, and lower than 0.3 near ice caps. This ratio does not depend on the load thickness or density. This ratio is also fundamentally different than for many magmatic sources that can be approximated by a point source of pressure in an elastic half-space (the Mogi model). For the Mogi model, the ratio between lateral and vertical displacement, at horizontal distance r , is given by r/D_M where D_M is the depth of the magmatic source. Magmatic sources that induce surface deformation are usually localized at depth smaller than 10 km, which implies that, at a distance r from the magmatic source larger than 5 km, the ratio between lateral and vertical displacement is larger than 0.5. In Iceland, shallow magma chamber are at a much shallower depth, around 3 km for some of the most active volcanoes (Sturkell *et al.* 2006; Sigmundsson 2006; Gudmundsson *et al.* 1994), implying an even larger value for the ratio between lateral and vertical displacement.

2.4 Temporal evolution of displacement

The preceding analysis gives the initial and final relaxed response to surface loads. At intermediate times, the deformation is characterized by transition from the initial to the final relaxed state. In the case of a Newtonian viscosity, this relaxation process is associated with an exponential decay of displacement rates. In general, a load needs to be decomposed into its spectral components, and decay of each spectral component needs to be evaluated (Fourier analysis). A load spectral component of wavelength λ placed on the surface of a Newtonian viscous half-space will cause vertical surface displacement given by (e.g. Turcotte & Schubert 2002):

$$U_z \propto e^{-t/t_R} \quad (14)$$

where the relaxation time t_R is given by:

$$t_R = \frac{2\eta k}{\rho_f g} \quad (15)$$

where η is the dynamic viscosity, ρ_f is the fluid density, g is acceleration of gravity and k is the wave number, equal to $2\pi/\lambda$. A disc load placed on Newtonian viscous half-space will cause relaxation that decays in a similar manner as the equation above, with the wave number k being replaced by an effective wave number for the load. The effective wave number for a disc load can be approximated as to $1.2/R_o$, where R_o is the radius of a disc load (Cathles 1975, p. 325). The effect of an elastic plate lying on the viscous half-space is to increase the rate of decay of short wavelengths (Cathles 1975, appendix VI). For the case of a thin elastic plate, the relaxation time becomes:

$$t_R = \frac{2\eta k}{\rho_f g + k^4 D} \quad (16)$$

where D is the flexural rigidity of the plate.

In our models, we assume that transition from an initial to final relaxed state is dominated by a similar process as described above, characterized by displacements with an effective relaxation time t_R . Then, for a given distribution of load, the description of the deformation field is:

$$U_z(r, t) = (U_z^\infty(r) - U_z^H(r))e^{-t/t_R} + U_z^H(r) \quad (17)$$

Eqs (15) and (16) represent simplifications, where an elastic uppermost layer is ignored, or assumed to be thin. In more realistic case, its finite thickness has to be considered. For a given viscosity, we estimate the corresponding relaxation time by comparing the predicted deformation using eq. (17) with deformation induced by

a disc load on an elastic plate lying above a viscous medium. We use a solution given by Sigmundsson (1990), considering an arbitrary thickness of the elastic plate. Taking $R_o = 14$ km appropriate for Mýrdalsjökull ice cap, an elastic thickness of 5 km and $\rho_f = 3100 \text{ kg m}^{-3}$, a viscosity of 4 to $10 \times 10^{18} \text{ Pa s}$ (as estimated for Vatnajökull Pagli *et al.* 2005, 2006), we derive an effective relaxation time of 120 to 300 yr. Eq. (15) for a viscous half-space would give a larger relaxation time, in the range of 700–1800 yr.

We expect the horizontal and vertical displacements to decay with the same effective relaxation time. The displacement is obtained by time-space convolution of the Green functions (see the appendix).

3 DEFORMATION OF THE KATLA VOLCANO

The Katla subglacial volcano in South Iceland is one of three most active volcanoes in Iceland, with 20 documented eruptions in the last 1100 yr (Larsen 2000). It has a caldera that is filled with ice over 600 m thick, located under the Mýrdalsjökull ice cap (Björnsson *et al.* 2000). Katla eruptions are phreatomagmatic, associated with major ice melting and jökulhlaups (sudden glacial outburst floods), and are therefore particularly hazardous. Deformation around Katla has been monitored since the 1960s when three optical levelling tilt stations in the area were installed (Tryggvason 1973). A local GPS network was installed at the volcano in the 1990s and later expanded (Sturkell *et al.* 2003). In 1999, two continuous GPS stations were installed near the edge of Mýrdalsjökull ice cap and one at the nearby Eyjafjallajökull glacier, as a part of country-wide network of continuous GPS stations in Iceland (Geirsson *et al.* 2006). Satellite radar interferograms based on data acquired by the ERS-1 and ERS-2 missions covering Katla and surrounding have also been formed as a part of a larger study of deformation in South Iceland (Pedersen 2004). However deformation signals in the surroundings of Mýrdalsjökull ice cap are small, and have not been separated from atmospheric noise. The current geodetic network is shown in Figs 5 and 6. Detailed results from this geodetic network are presented by Sturkell *et al.* (2006). From 1999 to 2004 the deformation is characterized by uplift and expansion across the Katla volcano and the Mýrdalsjökull

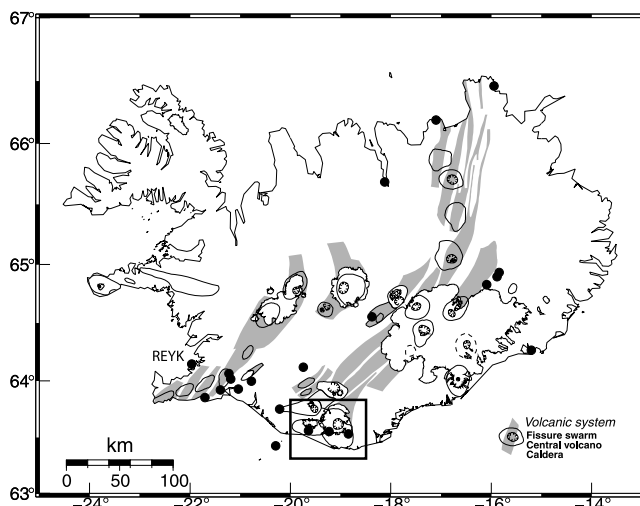


Figure 5. Continuous GPS stations (dots) and tilt station (crosses) in Iceland. The Reykjavik (REYK) reference station is reported. Volcanic zones of Iceland are reported (from Einarsson & Saemundsson 1987). The studied area (Figs 6 and 15) is outlined in black.

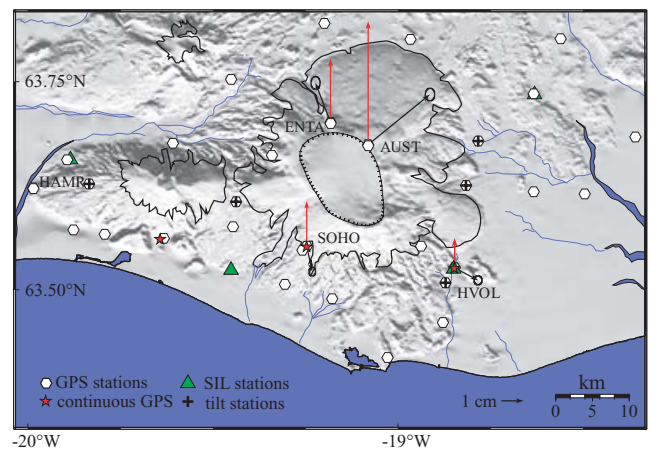


Figure 6. Displacement around Katla, June 2001 to June 2004. Observations at stations AUST, ENTA, SOHO and HVOL are relative to HAMR. The black arrows signify horizontal motion and the red arrows denote vertical movement. Outline of icecaps are shown. Geodetic network around Katla volcano and Mýrdalsjökull ice cap is reported.

ice cap (Figs 6 and 7). Uplift rates at AUST station at Katla amount to up to 2 cm yr^{-1} . Horizontal displacements are mostly aligned away from the volcano/icecap, with rates up to 1 cm yr^{-1} . Fig. 8 shows the ratio between the horizontal and the vertical displacements observed at GPS stations around Mýrdalsjökull compared to the values expected from the Mogi point source model for the magma accumulation and the ice load effect (see chapter 2.3). Ice load change cannot account for the whole displacement measured around Katla volcano (because the observed ratios are larger than the expected value considering only a loading effect). In order to explain this displacement we have to consider an intrusion of magma beneath the volcano as discussed by Sturkell *et al.* (2006).

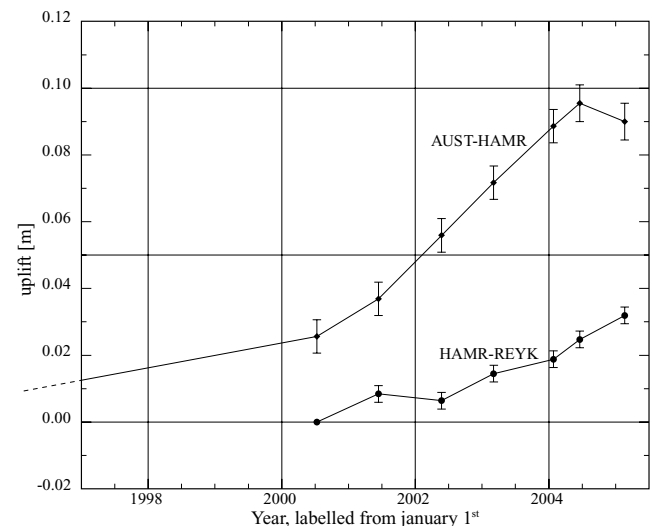


Figure 7. Uplift of AUST relative to HAMR reference station from 1997 to 2005. The line before 2000 is obtained with one earlier observation recorded in 1992 and reflects the average displacement between 1992 and 2000. Also shown is the inferred uplift from 2000 to 2005 of the HAMR reference station relative to a continuous GPS stations far away in Reykjavik (REYK shown in Fig. 5). About half of the HAMR–REYK relative uplift is due to subsidence of the REYK station in a global reference frame of 3 mm yr^{-1} (Sella *et al.* 2002).

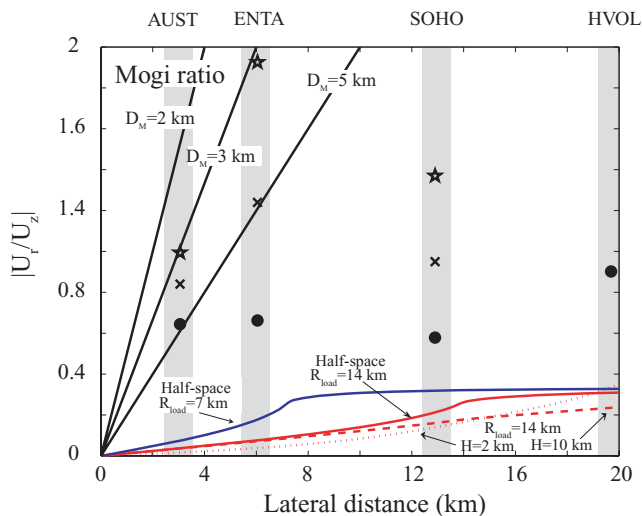


Figure 8. Ratio between the modulus of the horizontal and the vertical displacements as a function of lateral distance. Black curves are for the displacement induced by a Mogi source located at different depth (2, 3 and 5 km), red curves are for the displacement induced by a 14 km radius disc load (continuous line for half-space, dashed line for $H = 10$ km and dotted line for $H = 2$ km) and the blue curve is for the displacement induced by a 7 km radius disc load applied on a half-space. Value of E is 29 GPa. Values observed at GPS stations between 2001 and 2004 are shown (filled circles) versus their lateral distance from the centre of the caldera. The ratio values corrected from the ice load effect are reported: crosses correspond to the elastic half-space correction (see Fig. 12) and stars are obtained with the temporal model shown in Fig. 14.

The continuous GPS measurements reveal an annual cycle in coordinate values, superimposed on a linear change in east, north, and vertical components (Fig. 9). Annual fluctuations, modelled with a function of the form $A \cos(\omega t + \phi)$, where A is amplitude, ω is equal to $2\pi/\text{year}$, and ϕ is a phase angle, occur to some extent for coordinates of all the continuous GPS stations in Iceland (Geirsson *et al.* 2006). They may partly be an artefact due to improper consideration of atmospheric effects in data processing, or be a real Earth response to cryospheric loading. An annual fluctuation in east components in coordinate values relative to the REYK reference station has furthermore been suggested to originate mostly from an annual cycle in the east movement of the REYK reference station itself. Despite these limitations, the annual cycle in coordinates of the SOHO station relative to the REYK reference station is exceptional (Fig. 9a). Its amplitude is 1.4 mm in east, 1.6 mm in north, and 5.2 mm in vertical components (Geirsson *et al.* 2006). In the vertical SOHO has the second largest amplitude of all continuous stations in Iceland (with a maximum of observed subsidence at the beginning of June); in the north component it has the largest observed amplitude (more than 40 per cent larger than for all other sites, the maximum being observed at the end of April). Considering the size of the annual amplitudes at SOHO, we expect majority of these fluctuations to be real and reflect cryospheric loading. For the other continuous GPS site near the Mýrdalsjökull ice cap, the HVOL station (Fig. 9b), the amplitudes of the annual cycle are 1.1, 1.1 and 4.9 mm yr^{-1} in east, north and vertical components. Maximum subsidence occurs at the end of May and the maximum in the north component is reached in late April.

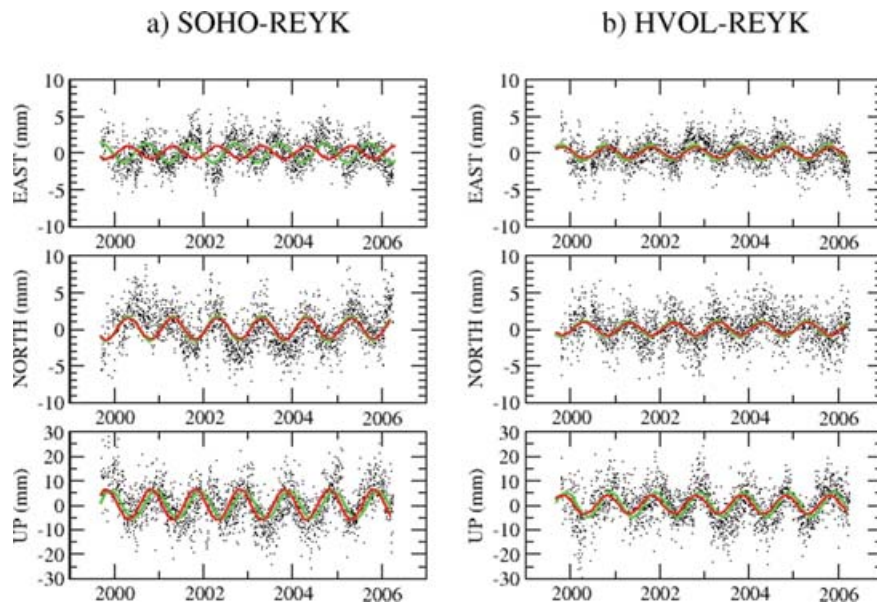


Figure 9. Time-series of east, north and vertical component of the SOHO and HVOL GPS stations (reference station is REYK). The linear trend (for SOHO, respectively 16.63 mm yr^{-1} , -8.08 mm yr^{-1} and 10.11 mm yr^{-1} for the east, north and vertical component; for HVOL, respectively 18.98 mm yr^{-1} , -6.94 mm yr^{-1} and 8.51 mm yr^{-1} for the east, north and vertical component) has been removed. The green curve is a fit of data by a function $A \cos(\omega t + \phi)$ (for SOHO, the phase ϕ is respectively 1.73, -2 and 0.42 for east, north and vertical component; for HVOL ϕ is, respectively, 1.30, -1.94 and 0.57 for east, north and vertical component). The red curve is for the elastic model (see Fig. 11) considering a maximum of ice thickness at the beginning of May.

4 DEFORMATION INDUCED BY VARIATIONS OF ICE LOAD AT MÝRDALSJÖKULL

4.1 Ice thickness variations at Mýrdalsjökull: an annual cycle superimposed on a long-term decrease

Katla volcano is the best monitored volcano in Iceland. One component of the monitoring program is airplane radar measurements of ice surface elevation (absolute uncertainty 2–3 m, relative uncertainty about 1m, Gudmundsson *et al.*, 2007). The aim of these measurements is to detect changes in ice volume, in particular to locate areas of increased geothermal heat at the volcano. Since 1999 measurements have been conducted at least twice every year. The measurements have revealed the following: (1) a gradual retreat has occurred at the glacier termini, and (2) an annual cycle in glacier elevation occurs within the Katla caldera, the highest part of the Mýrdalsjökull ice cap.

A map of ice thickness variation observed at Mýrdalsjökull between October 1999 and October 2004 was produced based on airplane radar measurements (Fig. 12a). The ice thickness has clearly decreased over this period of time and this decrease is restricted to the marginal areas of the glacier. This retreat is a response to warm climate; melting near the termini exceeds ice transport down the outlet glaciers. The map (Fig. 12a) only shows the total change in a 5 yr period but the ablation takes place mainly in the period May–September. It follows that this ice thickness evolution at each location can be described as a linear trend characterized by a slope a (in m yr^{-1} , this slope is the value of Fig. 12a divided by 5 yr) and an annual cycle of amplitude $a/2$. Although the ice thickness has not changed in the central part of the ice cap, an annual cycle occurs within the Katla caldera. It is due to accumulation during winter time and melting during summer of the superficial layer of snow. The amplitude (maximum to minimum) of this cycle is 6–10 m (Fig. 10).

4.2 Elastic modelling of seasonal effect

The annual ice load cycle is modelled in what follows as a disc load of variable thickness in the central part of the caldera (Fig. 11a),

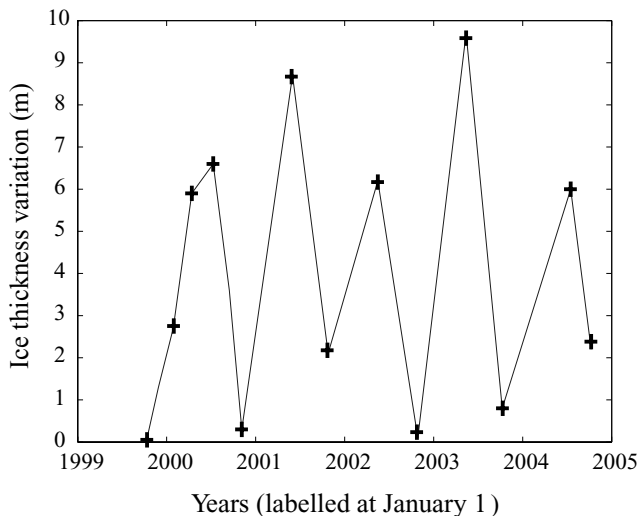


Figure 10. Ice fluctuation: observed time-series within the Katla caldera. Measurements are shown by crosses.

as well as a contribution from the average thinning measured between 1999–2004 (Fig. 12a). Snow accumulation is by far most pronounced within the Katla caldera, and we assumed an annual firm variation there of 6.5 m (maximum to minimum). Snow accumulation decays rapidly away from this central area. We model this rapid decay as a peripheral area of 2.4 km width surrounding the area of the main annual snow load, with half the snow load of central area (see Fig. 11a). We consider a density of 650 kg m^{-3} for this snow. In addition to this, we take into account the contribution to annual load cycle from uneven long-term thinning of the ice cap. Yearly average thinning in the 1999–2004 period is considered (Fig. 12a). An amplitude (maximum to minimum) equal to half the thinning per year is considered as a contribution to the annual load variation with ice density set to 900 kg m^{-3} . We modelled both contributions as a sinusoidal function with an amplitude being the sum of the two contributions we fixed the maximum ice thickness to occur the beginning of May. We used this model for annual load variations at Mýrdalsjökull to calculate expected annual variation in deformation fields. Considering the short time period of the signal, we assumed a purely elastic behaviour. Predicted vertical displacements were then compared to the vertical annual signal measured at two continuous GPS stations at the edge of Mýrdalsjökull, in order to constrain the value of the effective Young's modulus, E , under the ice cap. The records from GPS stations SOHO and HVOL favour respective values for E of 35.3 GPa and 22.7 GPa in order to fit the data. Based on these values we conclude that the value of E is 29 ± 5 GPa for the Mýrdalsjökull area. An error of 1 mm in the determination of the amplitude of the vertical variation induces an error in the estimate of E smaller than 5 GPa. The calculated signal, considering a Young's modulus of 29 GPa, is shown in Fig. 9 for the observed time-series from GPS stations SOHO and HVOL. The phase delay for the vertical displacement is smaller than 1.2 month. A reasonable fit is observed for the north and vertical components. Figs 11(b)–(d) show the resulting elastic response expected for the seasonal effect with a Young's modulus of 29 GPa.

Our present estimation of E is based on the assumption that the vertical component of annual displacement measured at SOHO and HVOL is entirely due to ice-loading variation occurring at Mýrdalsjökull which is the closest ice cap. However, part of this signal could be caused by seasonal change at other ice caps (Eyjafjallajökull, Vatnajökull). Even snow load outside the ice cap might influence the displacement at the stations we used. Our model may therefore underestimate the load amplitude. For instance, if we add the effect of a seasonal load variation at Vatnajökull ice cap modelled by a 50 km radius disc load of 1.5 m ice, the inferred value of E becomes 50 GPa. Grapenthin *et al.* (2006) derived the values of 40 ± 15 GPa for the Young's modulus based on a comparison of seasonal variations in Icelandic continuous GPS stations and the predicted displacements induced by annual snow load on Iceland's four largest ice caps. Furthermore, part of the observed cyclic signal in the continuous GPS data could be an artefact due to atmospheric effects. It follows that the value of 29 GPa has to be considered as a minimum value. Using a minimum value for E in the following calculations give us an upper limit for estimated displacements. Despite uncertainties, a consideration of the seasonal effect appears to be the best way to constrain E as it is a short-term effect and therefore the response is expected to be elastic throughout the underlying Earth structure. This seasonal effect is largest at the centre of the ice cap and its lateral extension is smaller than the extension of the long-term signal induced mostly by ice thinning at the edge of Mýrdalsjökull.

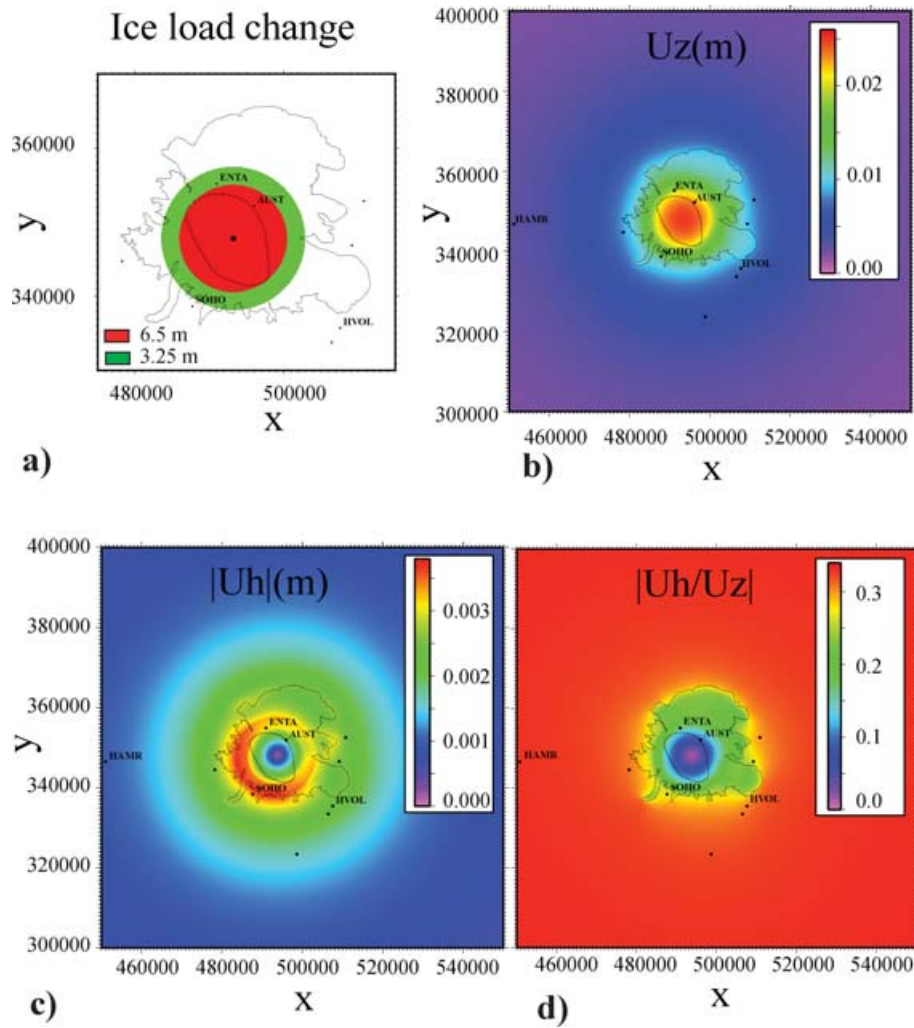


Figure 11. Elastic response to a seasonal load at Mýrdalsjökull. Both the annual snow thickness changes occurring in the central part (a) and the apparent annual cycle induced by the long-term retreat at the glacier edges (Fig. 12a) are considered for calculation. (a) Model used for the annual snow thickness change in the central part of Mýrdalsjökull is a uniform disc load (centre at $x = 493225$, $y = 347804$ Lambert coordinates) with radius 7.2 km and thickness 6.5 m. It is surrounded by a 2.4 km wide zone with half this thickness change. Density $\rho_{\text{ice}} = 650 \text{ kg m}^{-3}$ is assumed. (b) Vertical displacement (U_z expressed in m.) (c) Modulus of the horizontal displacement ($|U_h|$ expressed in m.) (d) Ratio between horizontal and vertical displacement ($|U_h/U_z|$). Poisson's value ν is fixed at 0.25 and the Young's modulus at 29 GPa. Black dots show location of GPS and tilt stations. Limit of the Katla caldera and outline of Mýrdalsjökull are also shown.

4.3 Influence of long-term ice thinning

Fig. 12 shows the inferred instantaneous elastic displacement induced by the ice loss measured between 1999 and 2004 whereas Fig. 13 shows the inferred final 'relaxed' amount of displacement induced by the ice loss.

As expected the displacements are much larger for the relaxed state than for the instantaneous response, for the vertical displacement there is a factor of 10 between the two end-members. In both cases, for regions more than 10 km away from the ice cap edges, the effect is axisymmetrical and quite similar to the one induced by a circular load. On the contrary, close to the glacier outline, where most of the GPS stations are located, the displacement field depends strongly on the local ice load distribution which justifies the need of a model based on integration of Green's functions. The consideration of the correct spatial load distribution becomes more important for smaller elastic thickness. The value of the Young's modulus mainly influences the amplitude of the displacement: a minimum value for E gives us a maximum estimate of the displacement.

Displacements induced by gradual ice thinning can be expected to be a combination of the instantaneous elastic response and a part of the final state as discussed in chapter 2.4. Making the assumption that Mýrdalsjökull thinned at a constant rate \dot{a} during the last τ_o years and using eq. (A3) the current vertical displacement rate is given by

$$\dot{U}_z(r) = \dot{a}(e^{-\tau_o/t_R} - 1) \int_R [U_{zG^\infty}(\vec{r} - \vec{r}') - U_{zGH}(\vec{r} - \vec{r}')] \times \rho(\vec{r}')e(\vec{r}') d\vec{r}' + \dot{a} \int_R U_{zG^\infty}(\vec{r} - \vec{r}')\rho(\vec{r}')e(\vec{r}') d\vec{r}' \quad (18)$$

where $U_{zG^\infty}(r)$ and $U_{zGH}(r)$ are the Green's function corresponding to a unit point mass.

The maximum displacements are achieved for the relaxed state (displacements shown in Fig. 13 for a 5 yr period). It corresponds to the case where ice has been thinning at the same rate for a long time or the relaxation time is very small ($\tau_o \rightarrow \infty$ or $t_R \rightarrow 0$). The minimum value is the instantaneous elastic response (displacements

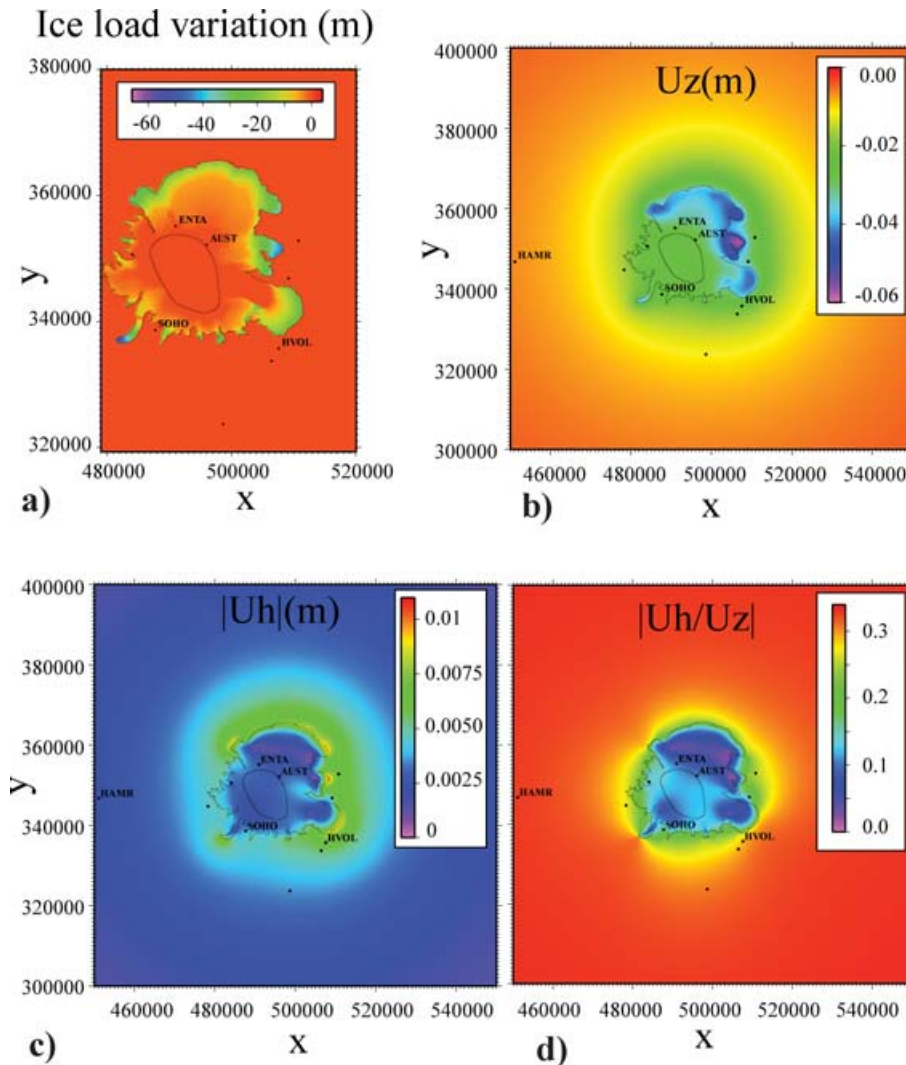


Figure 12. Elastic response to the long-term ice thinning at Mýrdalsjökull. (a) Model used for the ice elevation change at Mýrdalsjökull between October 1999 and October 2004 (density of ice is set to $\rho_{\text{ice}} = 900 \text{ kg m}^{-3}$). (b) Vertical displacement (U_z expressed in m). (c) Modulus of the horizontal displacement ($|U_h|$ expressed in m). (d) Ratio between horizontal and vertical displacement ($|U_h/U_z|$). Poisson's value ν is fixed at 0.25 and $E = 29 \text{ GPa}$. Black dots show location of GPS and tilt stations. Limit of the Katla caldera and outline of Mýrdalsjökull are also shown.

shown in Fig. 12 for a 5 yr period) and is reached in the case the thinning effect is beginning or the relaxation time is very large ($\tau_o \rightarrow 0$ or $t_R \rightarrow \infty$). When $\tau_o = t_R$ the effect is almost the relaxed effect scaled by 0.6.

We calculated the expected current rate of displacement, assuming the Mýrdalsjökull ice cap has thinned the same way during the last 115 yr. This is the interval of general ice retreat at Icelandic glaciers. After being at a maximum advance in the 19th century, the glaciers started to retreat around 1890. The rate of thinning is obtained by dividing the ice elevation change observed between 1999 and 2004 by 5 yr (Fig. 14a). This is a rather rough approximation of long-term ice load history at Mýrdalsjökull but it allows us to estimate an order of magnitude of the expected ongoing displacement field in response to past ice reduction. Calculations are done with an elastic thickness of 5 km. E is taken equal to 29 GPa as estimated by modelling of seasonal effect (4.2). In order to obtain a model that matches the observations (an uplift rate around the ice cap close to 4 mm per year), a very high relaxation time of about 7000 yr has to be considered. As discussed later, it may be an overestimate. Results

are shown in Fig. 14. Many parameters can be adjusted that influence the amplitude of the uplift rate, among them the elastic thickness, the elasticity parameters (E and ν), the history of ice loading and the mantle viscosity. From eq. (15), a relaxation time of 7000 yr would correspond to a viscosity of $3.9 \times 10^{19} \text{ Pa s}$. This viscosity is already four times larger than the value inferred at Vatnajökull ice cap (Pagli *et al.* 2005, 2006). By comparing with the solution for a 14 km radius disc load applied on an elastic plate lying over a viscous medium derived from Sigmundsson (1990), the corresponding viscosity would be $2.5 \times 10^{20} \text{ Pa s}$. Deformation rates of the same order of magnitude as the one shown in Fig. 14 would be produced with a smaller viscosity if we increase the Young's modulus (as our estimation is a minimum value), increase the plate thickness H or reduce the ice thinning.

The corresponding expected displacements between 2001 and 2004 at GPS stations AUST, ENTA, SOHO and HVOL relative to HAMR are shown in Fig. 15(a) for comparison with the observed displacement field (Fig. 6). We can note that vertical displacement at the four stations are the same order of magnitude ($\approx 12 \text{ mm}$ at the

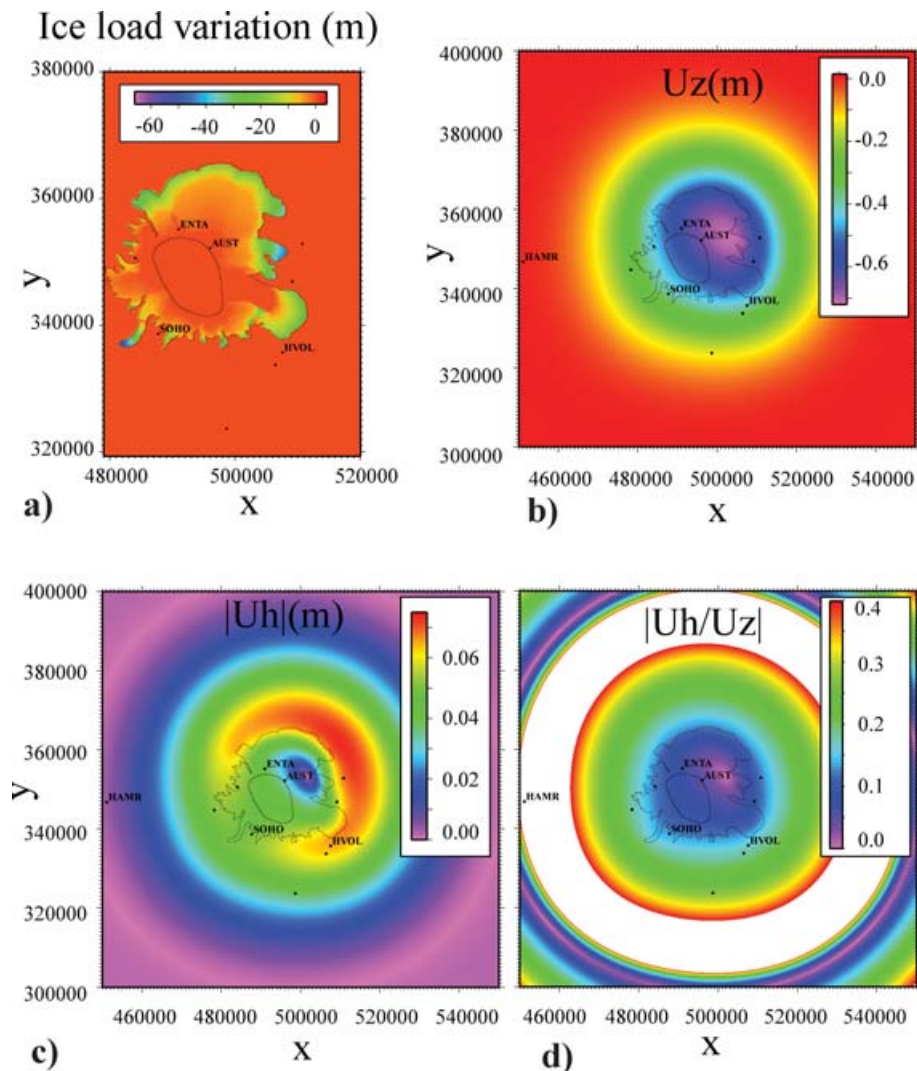


Figure 13. Final (relaxed) state of displacements corresponding to the ice thinning observed at Mýrdalsjökull between 1999 and 2004. Calculations are obtained considering a 5 km thick elastic plate lying above an inviscid fluid. (a) Model used for the ice elevation change at Mýrdalsjökull between 1999 October and 2004 October (density of ice is set to $\rho_{\text{ice}} = 900 \text{ kg m}^{-3}$). (b) Vertical displacement (U_z expressed in m.) (c) Modulus of the horizontal displacement ($|U_h|$ expressed in m.) (d) Ratio between horizontal and vertical displacement ($|U_h/U_z|$). Poisson's value ν is fixed at 0.25 and $E = 29 \text{ GPa}$, a mantle density of $\rho_f = 3100 \text{ kg m}^{-3}$ is assumed. Black dots show location of GPS and tilt stations. Limit of the Katla caldera and outline of Mýrdalsjökull are also shown.

edge of the ice cap (SOHO and HVOL) and $\approx 18.5 \text{ mm}$ inside the cap (AUST and ENTA)) so that the residuals between observations (Fig 6) and ice unloading model (Fig. 15a) shown in Fig. 15(b) have a strong gradient with distance from the caldera centre. Horizontal displacements induced by ice unloading are small ($\approx 1 \text{ mm}$ except for HVOL where it reaches 5 mm) resulting in large horizontal displacements for the residuals (Fig. 15b). Correcting the observed displacements for the ice unloading effect results in increased values for the ratio between the size of horizontal and vertical displacement as shown in Fig. 8. The new ratio obtained is consistent with a magmatic source located at about 3 km depth for the two closest stations (AUST and ENTA).

5 DISCUSSION

In chapter 4.2 we inferred a 'static' value of Young's modulus around Mýrdalsjökull ice cap from a comparison between continuous GPS data and the seasonal ice load variations. Most estimates of the

Young's modulus for the Earth rest on analysis of seismic velocities and density variation, giving an estimate of the 'dynamic' value of E . For Iceland, a profile of the dynamic Young's modulus derived by Gudmundsson (1988) based on a crustal model by Pálmason (1971), shows variation in dynamic E from 14 GPa at the Earth's surface to 57 GPa at $\sim 4 \text{ km}$ depth. Values in the range of 100–130 GPa are reached at a greater depth. Comparable values for the dynamic E are obtained from consideration of a new seismic velocity model for Iceland of Allen *et al.* (2002). Following the suggestion of Cheng & Johnson (1981) regarding the difference in the dynamics and static values, Gudmundsson (1988) applied a static Young's modulus equal to half the value of the dynamic Young's modulus. From laboratory measurements in undamaged rocks (Eissa & Kazi 1988), values of static Young's moduli appear on the other hand to be only 5 to 10 per cent lower than those of dynamic moduli. However this relation is still poorly constrained and could be quite different in case of in-situ, damaged rocks. Some attempts to constrain the static value of Young's modulus in volcanic areas are based on comparison

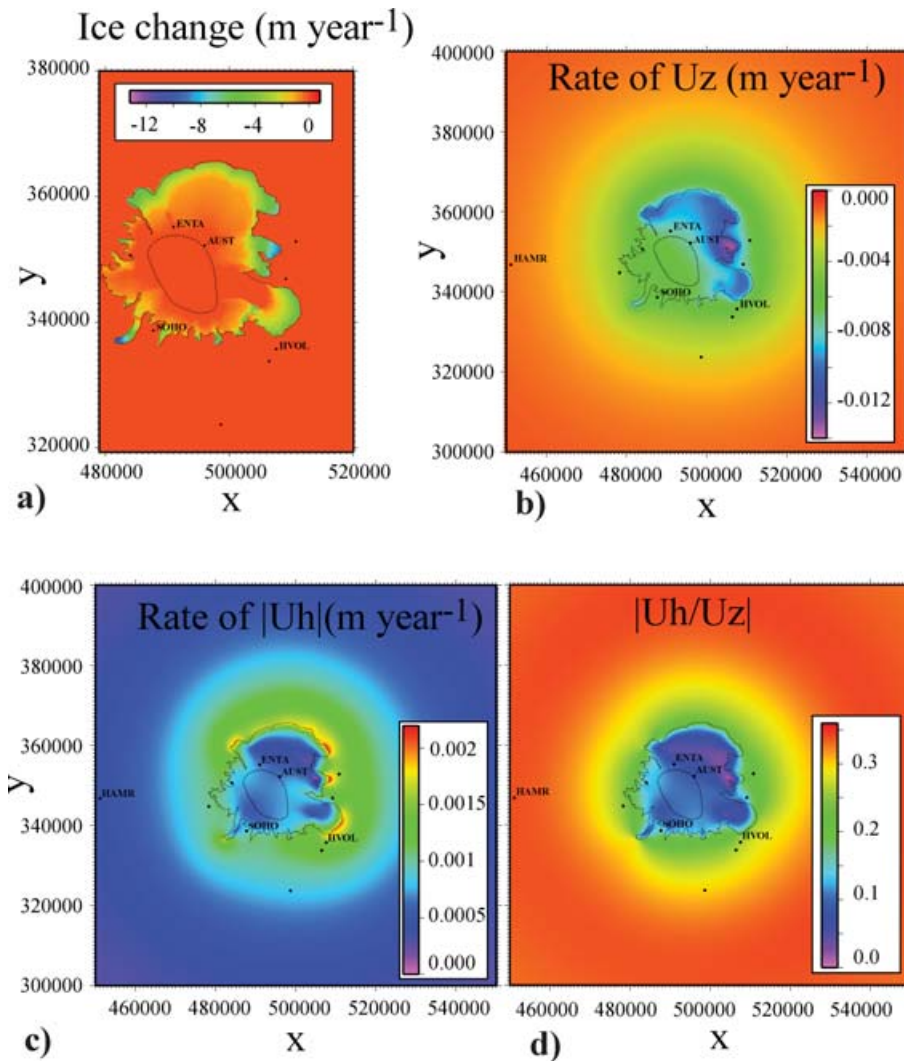


Figure 14. Inferred rate of current displacement resulting from the past 115 yr of ice thinning at a constant rate equal to that in the period 1999–2004. Calculations are obtained considering a 5 km thick elastic plate. The relaxation time is fixed at 7000 yr, Poisson's value ν is fixed at 0.25 and $E = 29$ GPa. Value for the mantle density is fixed to $\rho_f = 3100 \text{ kg m}^{-3}$. a) Model used for the annual rate of ice elevation change at Mýrdalsjökull during the last 115 yr (density of ice is set to $\rho_{\text{ice}} = 900 \text{ kg m}^{-3}$). b) Vertical displacement (U_z expressed in m yr^{-1}) c) Modulus of the horizontal displacement ($|U_h|$ expressed in m yr^{-1}) d) Ratio between horizontal and vertical displacement ($|U_h/U_z|$).

between mechanical models and observations (dyke sizes (Rubin & Pollard 1987), deformation data (Beauducel *et al.* 2000)). A static value of 3 ± 2 GPa is often used in mechanical models for volcanic areas (Cayol & Cornet 1998; Pinel & Jaupart 2004), which corresponds to a ratio of static versus dynamic value close to 0.25 (Cayol & Cornet 1998). In the case of Mýrdalsjökull, such low values are excluded based on the analysis in chapter 4.2. A value of E equal to 3 GPa would lead to an annual cycle in deformation one order of magnitude larger than observed (that fits $E = 29$ GPa).

The method to infer deformation due to load changes presented in this paper is general and we use some geodetic data from Katla volcano as an example for its application. With the Earth and ice-loss models used, the area where ongoing deformation occurs extends some tens of kilometers outside the ice cap edge. In our case, the HAMR GPS reference station is, however, outside the significantly deforming area due to ice load change at Mýrdalsjökull (Figs 11–14). It may on the other hand be influenced by deformation due to ice load change or magma movements at the neighbouring Eyjafjallajökull volcano, which are not considered in our model. The

model predictions displayed in Fig. 14 depend on the ice-loss model for retreat last century and the parameters of the Earth model used for calculation, both of which are uncertain. The ice-loss model for past century is particularly simple and assumes same thinning rates in last century as in 1999–2004. Although this is an oversimplification, it clearly demonstrates that vertical displacement rates around the ice cap due glacio-isostatic response may be on the order of cm yr^{-1} , but horizontal movements are expected in range of only few mm yr^{-1} . An improved model for ice loss during last century together with more extensive geodetic data will allow further constraints to be derived on the Earth model parameters. The geodetic data to consider include some GPS data as well as the long time-series of ground tilt inferred from optical leveling at several sites in the area since the 1960s (Tryggvason 1973, 2000). These tilt series may contribute to the understanding of the annual cycle in deformation as originally suggested by Tryggvason (1973), but more frequent observations are needed each year for this purpose. These tilt data also suggest small long-term rate of tilt ($< 0.3 \mu\text{rad yr}^{-1}$), which is the same order of magnitude as the tilt expected from the model

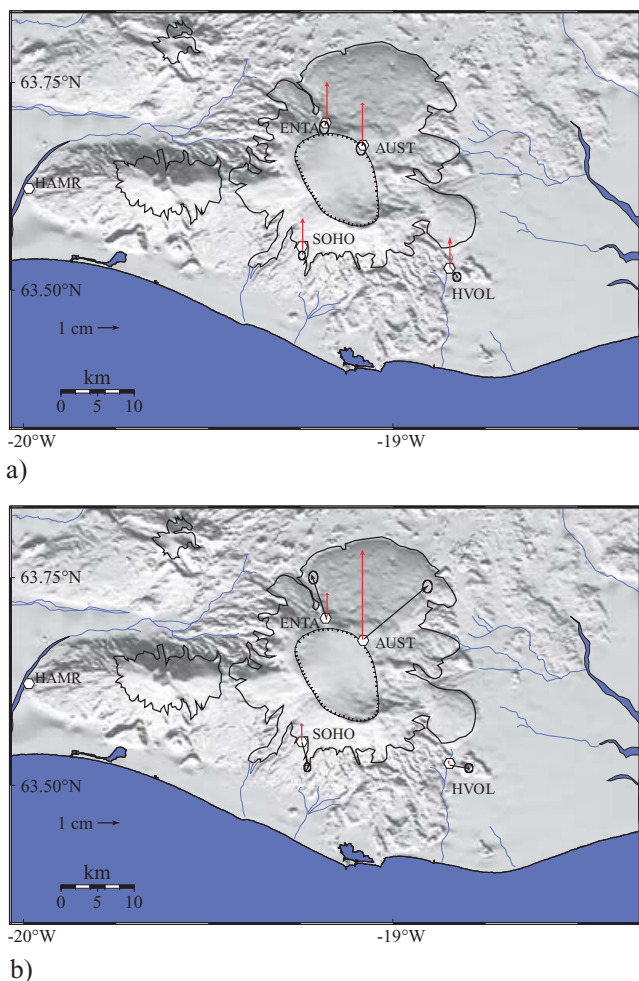


Figure 15. Predicted displacements induced by ice unloading around Katla from 2001 June to 2004 June. Uplift (red arrows) and horizontal displacement (black arrows) are shown at AUST, ENTA, SOHO and HVOL relative to HAMR. (a) Model of ice unloading (parameters used are the same as in Fig. 14). (b) Difference between displacements observed (see Fig. 6) and the ice unloading model. Outline of icecaps are shown.

presented in Fig. 14. Vertical displacement rate at the centre of ice cap according to that model vary from about 1 cm yr^{-1} near the centre of the ice cap, to zero at a distance of about 30 km, corresponding to tilt of about $0.33 \mu\text{rad yr}^{-1}$. However this result has been obtained using an eventually overestimated value for mantle viscosity ($2.5 \times 10^{20} \text{ Pa s}$). Similar deformation rates can also be produced using lower viscosity if ice loss is reduced (scales down the amplitude of the uplift) or Young's modulus is increased. If the amplitude of ice loss is reduced by a factor 2 or if Young's modulus is increased by a factor of 2, a good fit to data is obtained with a viscosity divided by 5. It may be justified to increase Young's modulus as our inferred value is a lower bound, and the details of the ice unloading history are uncertain. Considering both effects, it is possible to reconcile our results with a viscosity of the order of 10^{19} Pa s as estimated at Vatnajökull (Pagli *et al.* 2005, 2006). Increasing the elastic thickness also helps to slightly decrease the viscosity. Using an elastic thickness of 10 km (with $E = 29 \text{ GPa}$ and unchanged ice loss), a value of $2 \times 10^{20} \text{ Pa s}$ is suggested for mantle viscosity.

As discussed in Section 2.3, the ratio between horizontal and vertical displacements is useful to discriminate between displace-

ment induced by ice thinning and uplift induced by magma inflation at depth. Another way to discriminate such effects is to consider their wavelength. For a chamber shallower than 5 km, the vertical uplift induced at a lateral distance of 10 km will be at least 10 times smaller than the maximum uplift observed directly above the magmatic source. A magmatic source at shallow depth under Katla should not significantly affect vertical deformation outside the ice cap. On the other hand, the long-term thinning effect which is focused at the glacier edge induces displacements around the ice cap, and uplift in a more uniform manner over the central area. Based on the ratio argument and the lateral gradient of uplift observed at Katla, we can conclude that the deformation observed at Katla requires magma movements. Residuals shown in Fig. 15(b) imply a large lateral gradient and important horizontal displacements, which cannot be explained by the ice unloading effect. It is however clear that ice thinning can greatly influence parameters of magma sources (e.g. Mogi) inferred from inversion of geodetic data, if the ice-loading effect is ignored. Ratios between horizontal and vertical displacements measured at Katla and shown in Fig. 8 cannot be explained only by a Mogi model except for the station AUST. If we now consider that part of the uplift is due to the ice unloading effect, which has a small influence on the horizontal displacement, new displacement ratios obtained after correction are larger. Corrections have been done both considering a purely elastic effect (Fig. 12) and taking into account the viscous relaxation (Fig. 14). Corrected ratios are closer to the curves corresponding to a Mogi model. The errors arising from the neglect of loading effects depends on the data set used for the inversion: it will depend on the component of displacements used, the lateral extension of the network and the lateral distance to the reference station. At Katla, the ice-thinning effect has a larger wavelength than a shallow magmatic source. An inversion of vertical displacement only based on a Mogi point source that would not take into account the ice-thinning effect would tend to overestimate both the chamber depth and the volume of magma involved.

Our results show the relevance of using Green's function to model ice-loading effect at Katla where some knowledge about ice thickness exists, and most of the GPS stations are located near the edge of the evolving ice load. The effect of ice unloading is of great interest for Icelandic volcanoes but many other large strato-volcanoes are covered by glaciers that are currently retreating because of climate warming. Furthermore, the Green's function tool is potentially useful for any place where a local mass redistribution occurs. Such conditions are frequent in volcanic areas where large landslide or erupted products emplacement often take place and can be quantified using satellite data.

We only considered the deformation induced by ice unloading but large unloading events may induce large pressure change inside magma storage zone (Pinel & Jaupart 2005). Retreating ice cap may also induce changes of pressure conditions inside the plumbing system which in turn induces surface deformation. Studies on correlation between glaciation and eruptions rate have been carried out considering the loading effect either on magma generation conditions (Jull & McKenzie 1996) or on storage conditions (Sigvaldason *et al.* 1992; Jellinek *et al.* 2004).

Our indicators and modelling efforts of seasonal effects on land elevation at Katla volcano can also be compared to seasonal effects in seismicity. Katla volcano has for at least 40 yr shown a pronounced seasonal cycle in earthquake activity, with much more activity in the latter half of the year. Einarsson & Brandsdóttir (2000) point out that both the direct effect of ice load change and the resulting change in crustal pore pressure beneath the glacier could lead to seasonal

correlation of earthquakes. Comparing the two effects, both their likely size and phase, they conclude that the pore pressure effect is the more likely cause of the correlation at Katla. Such seasonal effects have been observed at other volcanoes as well; Christiansen *et al.* (2005) conclude that seasonal seismicity occurs at many of the western United States volcanic centres. Correlation of earthquake and magmatic activity with long-term and annual load changes is the task of a further study.

6 CONCLUSION

Measurements of crustal deformation fields on active volcanoes are of prime importance together with seismic monitoring, in order to understand magma movements. Ground inflation is a common indicator for magma flow towards shallow depth. However, many factors may influence the deformation signal recorded around volcanoes, including variation in surface loads that can be an important factor. In a general context of climate warming, this phenomenon may become important for ice covered volcanoes. Using observations and modelling of the Katla volcano, we show that knowledge of ice thickness evolution can be used to model displacements induced by ice load changes and identify its influence on the measured signal. This leads to better constraints on both the local crustal behaviour and the estimation of shallow magma movement.

ACKNOWLEDGMENTS

This study was supported by grants to enhance scientific cooperation between Iceland and France from the French Ministry for Foreign Affairs (EGIDE) and Jules Verne grant from the Icelandic Centre for Research. It was also supported by special grants from the Icelandic government for monitoring of the Katla volcano, additional support from the Icelandic Road Authority (Vegagerdin), and EU project VOLUME (Contract 18471). Critical reviews by M.P. Doin and an anonymous reviewer improved this paper.

REFERENCES

Allen, R.M. *et al.*, 2002. Plume-driven plumbing and crustal formation in Iceland, *J. geophys. Res.*, **107**(B8), 2072, doi:10.1029/2001JB000584.

Beauducel, F., Cornet, F.-H., Suhanto, E., Duquesnoy, T. & Kasser, M., 2000. Constraints on magma flux from displacements data at Merapi volcano, Java, Indonesia, *J. geophys. Res.*, **105**, 8193–8203.

Björnsson, H., Pálsson, F. & Gudmundsson, M.T., 2000. Surface and bedrock topography of Mýrdalsjökull, South Iceland: The Katla caldera, eruption sites and routes of jökulhlaups, *Jökull*, **49**, 29–46.

Brotchie, J.F. & Silvester, R., 1969. On crustal flexure, *J. geophys. Res.*, **74**, 5240–5252.

Cathles, L.M., 1975. *The Viscosity of Earth's Mantle*, Princeton University Press, Princeton, 386pp.

Cayol, V. & Cornet, F.H., 1998. Three-dimensional modeling of the 1983–1984 eruption at Piton de la Fournaise Volcano, Réunion Island, *J. geophys. Res.*, **103**, 18 025–18 037.

Cheng, C.H. & Johnson, D.H., 1981. Dynamic and static moduli, *Geophys. Res. Lett.*, **8**, 39–42.

Christiansen, L.B., Hurwitz, S., Saar, M.O., Ingebritsen, S.E. & Hsieh, P.A., 2005. Seasonal seismicity at western United States volcanic centers, *Earth planet. Sci. Lett.*, **240**, 307–321.

Comer, R.P., 1983. Thick plate flexure, *Geophys. J. R. astr. Soc.*, **72**, 101–113.

Einarsson, P. & Brandsdóttir, B., 2000. Earthquakes in the Mýrdalsjökull area, Iceland, 1978–1985: Seasonal correlation and connection with volcanoes, *Jökull*, **49**, 59–73.

Einarsson, P. & Saemundsson, K., 1987. *Earthquakes epicenters 1982–1985 and volcanic systems in Iceland, map*, in I hlutarins edli ed., Sigfusson, Th. I., Menningarsjóður, Reykjavík, Iceland.

Eissa, E.A. & Kazi, A., 1988. Relation between static and dynamic Young's moduli for rocks, *Int. J. Rock Mech. Min. Sci. and Geomech. Abstr.*, **25**, 479–482.

Geirsson, H. *et al.*, 2006. Current plate movements across the mid-atlantic ridge determined from 5 years of continuous GPS measurements in Iceland, *J. geophys. Res.*, **111**, B09407, doi:10.1029/2005JB003717.

Grapenthin, R., Sigmundsson, F., Geirsson, H., Arnadóttir, T. & Pinel, V., 2006. Icelandic rhythmicity: Annual modulation of land elevation and plate spreading by snow load, *Geophys. Res. Lett.*, in press.

Gudmundsson, A., 1988. Effect of tensile stress concentration around magma chambers on intrusion and extrusion frequencies, *J. Volc. Geotherm. Res.*, **35**, 179–194.

Gudmundsson, O., Brandsdóttir, B., Menke, W. & Sigvaldson, E., 1994. The crustal magma chamber of the Katla volcano in south Iceland revealed by 2-D seismic undershooting, *Geophys. J. Int.*, **119**, 277–296.

Gudmundsson, M.T., Högnadóttir, T., Kristinsson, A.B. & Gudbjörnsson, S., 2007. Geothermal activity in the subglacial Katla caldera, Iceland, 1999–2005, studied with radar altimetry, *Ann. Glaciol.*, in press.

Jellinek, A.M., Manga, M. & Saar, M.O., 2004. Did melting glaciers cause volcanic eruptions in eastern California? Probing the mechanics of dike formation, *J. geophys. Res.*, **109**, B09206, doi:10.1029/2004JB002978.

Jull, M. & McKenzie, D., 1996. The effect of deglaciation on the mantle melting beneath Iceland, *J. geophys. Res.*, **101**, 21 815–21 828.

Larsen, G., 2000. Holocene eruptions within the Katla volcanic system, south Iceland: Characteristics and environmental impact., *Jökull*, **49**, 1–28.

Pagli, C., Sigmundsson, F., Sturkell, E., Geirsson, H., Lund, B. & Arnadóttir, T., 2005. Ongoing glacio-isostatic crustal deformation around Vatnajökull ice cap, Iceland due to ice retreat: Observations and finite element modeling, *EOS, Trans. Am. geophys. Un.*, **86**, AGU Fall Meeting Abstracts, abstract G33A-0017.

Pagli, C., Sigmundsson, F., Lund, B., Geirsson, H., Sturkell, E., Einarsson, P. & Arnadóttir, T., 2006. Glacio-isostatic deformation around the Vatnajökull ice cap, Iceland induced by recent climate warming: GPS observations and finite element modelling, *J. geophys. Res.*, submitted.

Pálmason, G., 1971. *Crustal structure of Iceland from explosion seismology*, Soc. Sci. Iceland, XL, Reykjavík, Iceland, 187 pp.

Pedersen, R., 2004. Crustal deformation associated with the June, 2000, earthquakes in Southern Iceland and repeated magmatic intrusion in the Eyjafjallajökull volcano, 1994 and 1999, *PhD thesis*, University of Iceland.

Pinel, V. & Jaupart, C., 2000. The effect of edifice load on magma ascent beneath a volcano, *Phil. Trans. R. Soc. Lond.*, **A**, **358**, 1515–1532.

Pinel, V. & Jaupart, C., 2004. Magma storage and horizontal dyke injection beneath a volcanic edifice, *Earth planet. Sci. Lett.*, **221**, 245–262, doi:10.1016/j.epsl.2004.01.031.

Pinel, V. & Jaupart, C., 2005. Some consequences of volcanic edifice destruction for eruption conditions, *J. Volc. Geotherm. Res.*, **145**, 68–80, doi:10.1016/j.jvolgeores.2005.01.012.

Rubin, A.M. & Pollard, D.D., 1987. Origins of blade-like dikes in volcanic rift zones, In: Lipman, US Geological Survey Professional Paper **1350**.

Sella, G.F., Dixon, T. & Mao, A., 2002. REVEL: A model for recent plate velocities from space geodesy, *J. geophys. Res.*, **107**, doi: 10.1029/2000JB000033.

Sigmundsson, F., 1990. Viscosity of the Earth beneath Iceland; comparison of model calculations with geological data, *MSc. thesis*, University of Iceland, University press, 121 pp (in Icelandic with English summary).

Sigmundsson, F., 2006. *Iceland Geodynamics, Crustal Deformation and Divergent Plate Tectonics*, Praxis Publishing—Springer Verlag, Chichester, UK, 209 pp.

Sigmundsson, F. & Einarsson, P., 1992. Glacio-isostatic crustal movements caused by historical volume change of the Vatnajökull ice cap, Iceland, *Geophys. Res. Lett.*, **19**, 2123–2126.

Sigvaldason, G.E., Annertz, K. & Nielsson, M., 1992. Effect of glacier loading/deloading on volcanism: postglacial volcanic production rate of the Dyngjufjöll area, central Iceland, *Bull. Volcanol.*, **54**, 385–392.

- Sneddon, I.N., 1951. *Fourier transforms*, McGraw-Hill, 542 pp.
- Sturkell, E., Sigmundsson, F. & Einarsson, P., 2003. Recent unrest and magma movements at Eyjafjallajökull and Katla volcanoes, Iceland, *J. geophys. Res.*, **108**(B8), 2369, doi:10.1029/2001JB000917.
- Sturkell, E. *et al.*, 2006. Seismic and geodetic insights into magna accumulation at Katla subglacial volcano, Iceland: 1999 to 2005, *J. geophys. Res.*, submitted.
- Tryggvason, E., 1973. Surface deformation and crustal structure in the Myrdalsjökull area of South Iceland, *J. geophys. Res.*, **78**, 2488–2497.
- Tryggvason, E., 2000. Ground deformation at Katla: Results of precision levelling 1967–1995., *Jökull*, **48**, 1–8.
- Turcotte, D.L. & Schubert, G., 2002. *Geodynamics*, 2nd edn, Cambridge University Press, Cambridge.

APPENDIX A: TIME–SPACE CONVOLUTION OF THE GREEN’S FUNCTIONS

We call $h(\vec{r}, t)$ the ice load at position \vec{r} and time t , $\frac{\partial h}{\partial t}(\vec{r}, 0)$ is the load applied at $t = 0$ at position \vec{r} . From eqs (3), (13) and (17), the vertical displacement rate at a given time $t > 0$, induced by a given distribution of load applied at $t = 0$, is expressed by:

$$\frac{\partial U_z}{\partial t} = -\frac{1}{t_R} e^{-t/t_R} \int_R [U_{zG^\infty}(\vec{r} - \vec{r}') - U_{zGH}(\vec{r} - \vec{r}')] \times \rho(\vec{r}') \frac{\partial h}{\partial t}(\vec{r}', 0) dS(\vec{r}') \quad (\text{A1})$$

At $t = 0$, the displacement rate can be considered to be equal to the elastic instantaneous response, so that the general equation for the vertical displacement rate is given by:

$$\frac{\partial U_z}{\partial t} = -\frac{1}{t_R} e^{-t/t_R} \int_R [U_{zG^\infty}(\vec{r} - \vec{r}') - U_{zGH}(\vec{r} - \vec{r}')] \rho(\vec{r}') \frac{\partial h}{\partial t}(\vec{r}', 0) dS(\vec{r}') + \delta(t) \int_R U_{zG^\infty}(\vec{r} - \vec{r}') \rho(\vec{r}') \frac{\partial h}{\partial t}(\vec{r}', 0) dS(\vec{r}') \quad (\text{A2})$$

The rate of vertical displacement, at any time t , is obtained by convolution of eq. (A2) with the load history. In the case $h(\vec{r}, t) = e(\vec{r})a(t)$, t_R is a constant and this convolution is expressed by:

$$\dot{U}_z(\vec{r}, t) = -\frac{1}{t_R} \int_{-\infty}^{\infty} e^{-\tau/t_R} \dot{a}(t - \tau) \int_R [U_{zG^\infty}(\vec{r} - \vec{r}') - U_{zGH}(\vec{r} - \vec{r}')] \rho(\vec{r}') e(\vec{r}') dS(\vec{r}') d\tau + \int_{-\infty}^{\infty} \delta(\tau) \dot{a}(t - \tau) \int_R U_{zG^\infty}(\vec{r} - \vec{r}') \rho(\vec{r}') e(\vec{r}') dS(\vec{r}') d\tau \quad (\text{A3})$$

The two components (x, y) of the rate of the horizontal displacement are calculated in the same manner.